Erschienen in: Physical Review B ; 92 (2015), 17. - 174411
http://dx.doi.org/10.1103/PhysRevB.92.174411

PHYSICAL REVIEW B **92**, 174411 (2015)

Magnetic field control of the spin Seebeck effect

Ulrike Ritzmann, Denise Hinzke, Andreas Kehlberger, Er-Jia Guo, Mathias Kläui, and Ulrich Nowak
Department of Physics, University of Konstanz, D-78457 Konstanz, Germany
and Institute of Physics, Johannes-Gutenberg University Mainz, 55099 Mainz, Germany
(Received 29 April 2015; revised manuscript received 18 September 2015; published 9 November 2015)

The origin of the suppression of the longitudinal spin Seebeck effect by applied magnetic fields is studied. We perform numerical simulations of the stochastic Landau-Lifshitz-Gilbert equation of motion for an atomistic spin model and calculate the magnon accumulation in linear temperature gradients for different strengths of applied magnetic fields and different length scales of the temperature gradient. We observe a decrease of the magnon accumulation with increasing magnetic field and we reveal that the origin of this effect is a field dependent change of the frequency distribution of the propagating magnons. With increasing field the magnonic spin currents are reduced due to a suppression of parts of the frequency spectrum. By comparison with measurements of the magnetic field dependent longitudinal spin Seebeck effect in YIG thin films with various thicknesses, we find qualitative agreement between our model and the experimental data, demonstrating the importance of this effect for experimental systems.

DOI: 10.1103/PhysRevB.92.174411 PACS number(s): 75.76.+j, 75.30.Ds, 75.40.Mg

Spin caloritronics is an emerging research field promising spintronic devices with new functionalities, which rest on the combined transport of heat and spin [1,2]. A key tool that stimulated this field is the inverse spin Hall effect [3,4], which allows one to detect pure spin currents due to a transformation into measurable charge currents via spin-orbit coupling. Using this indirect measurement technique Uchida *et al.* measured the so-called spin Seebeck effect (SSE) [5]. The measurements showed that in the ferromagnetic insulator YIG a pure spin current is created due to an applied temperature gradient.

These findings triggered a variety of further studies in different groups [6–15] to investigate the origin of the detected spin currents. Interface effects due to a proximity effect which creates a magnetization in the normal metal were discussed [16], but various groups showed that the effect in the YIG/Pt system cannot be responsible for the measured signals [7,9,10,14]. A theoretical description of the magnonic spin Seebeck effect was developed by Xiao *et al.* [17]. With a two temperature model including the local magnon and phonon temperatures the measured spin Seebeck voltage was shown to originate from the local difference between magnon and phonon temperature at the Pt interface caused by thermal spin pumping. Later it was shown by spin model simulations that such a temperature difference can be caused by magnons traveling from the hotter towards the colder part of the sample [18]. By studying the thickness dependence of the SSE for thin YIG films, Kehlberger *et al.* [7] found an increasing spin Seebeck signal saturating above a critical length scale. This length scale can be referred to as the mean magnon propagation length. Similarly Agrawal *et al.* measured the time evolution of the SSE in the submicrosecond regime and explained their time dependent increase of the SSE by a dependence on the characteristic length scale of magnon propagation of a few hundred nanometers [12].

Further theoretical studies focused on the magnonic origin of the SSE [19,20] also predicting thickness dependent effects. Hoffman *et al.* [19] studied the SSE analytically within the framework of the stochastic Landau-Lifshitz-Gilbert equation. They assume that mainly magnons with $\hbar\omega \approx k_{\mathrm{B}}T$ contribute to the effect, but Boona *et al.* proposed that also subthermal magnons with lower energy can contribute or even dominate [21]. To reveal which magnons contribute to the effect, field dependent measurements that tailor the magnon spectrum are a key. Such measurements were made available in a recent publication by Kikkawa *et al.* [9] who studied the reduction of the SSE in the regime of high magnetic fields and report a suppression of the measured SSE signal. However, no theoretical explanation was given that reproduces the results completely and allows for a direct comparison of experiment and theory.

In this paper we study the influence of external magnetic fields on the SSE. Applying external fields manipulates the frequency distribution of the propagating magnons by increasing the frequency gap ω_{min} of the frequency spectrum. Therefore, the number of propagating magnons can be reduced by increasing the external magnetic field. We present numerical simulations of the magnon accumulation in linear temperature gradients and its dependence on external magnetic fields. For this study an atomistic spin model is used, which provides realistic spin wave spectra beyond parabolic approximation and without any artificial cutoff due to discretization effects. To understand the underlying physics, an analytical model is derived that explains the effect of the magnetic field within the framework of linear spin wave theory. Finally, our theoretical work is directly compared with field dependent SSE measurements of YIG thin films with different thicknesses, which cover a large range across the critical length scale showing good agreement.

For the numerical simulations we use an atomistic spin system consisting of localized spins with normalized magnetic moment $\mathbf{S}_i = \boldsymbol{\mu}_i/\mu_{\mathrm{s}}$ on a cubic lattice. Our model Hamiltonian $\mathcal{H}$ includes Heisenberg exchange interaction for nearest neighbors with exchange constant J, a uniaxial anisotropy with an easy axis in the z direction with anisotropy constant d_z, and an external field $\mathbf{B} = B_z\mathbf{e_z}$ parallel to the easy axis,

$$\mathcal{H} = -\frac{J}{2}\sum_{\langle i,j\rangle}\mathbf{S}_i\mathbf{S}_j - d_z\sum_i\left(S_i^z\right)^2 - \mu_{\mathrm{s}}B_z\sum_i S_i^z. \quad (1)$$

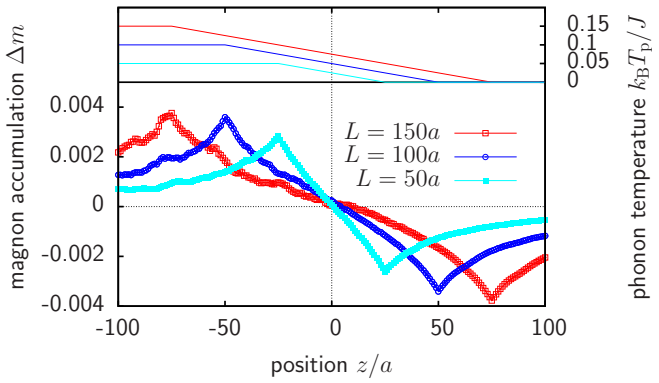

FIG. 1. (Color online) Local magnon accumulation Δm profile with the space position z in units of the lattice constant a for different thicknesses L.

The dynamics of each single spin are described by the stochastic Landau-Lifshitz-Gilbert (LLG) equation,

$$\frac{\partial \mathbf{S}_i}{\partial t} = -\frac{\gamma}{\mu_s(1+\alpha^2)}\mathbf{S}_i \times [\mathbf{H}_i + \alpha(\mathbf{S}_i \times \mathbf{H}_i)], \qquad (2)$$

consisting of a precession around its effective field $\mathbf{H}_i$ and a phenomenological damping with damping constant α [22,23]. γ is the gyromagnetic ratio and the effective field $\mathbf{H}_i$ is given by $\mathbf{H}_i = -\partial\mathcal{H}/\partial\mathbf{S}_i + \boldsymbol{\zeta}_i(t)$.

The temperature is included as additional noise term $\boldsymbol{\zeta}_i(t)$ in the effective field $\mathbf{H}_i$ fulfilling $\langle\boldsymbol{\zeta}(t)\rangle = 0$ and $\langle\zeta_i^\eta(0)\zeta_j^\theta(t)\rangle = 2k_B T_p \alpha\mu_s/\gamma\delta_{ij}\delta_{\eta\theta}\delta(t)$. The dynamics of the systems are studied by numerical integration of these equations using the Heun method [24].

In the systems considered, the temperature is spatially dependent, including a linear temperature gradient in the z direction with a constant slope over a distance L and two heat baths at the two ends of the system as shown in Fig. 1. The dimension of both heat baths is chosen to be large enough to minimize finite size effects in the area of the gradient. The given temperature profile describes the temperature of the phononic heat bath and it is assumed that the phonon temperature remains constant during the simulation. These classical simulations can be used for a qualitative comparison with the experimental measurements at room temperature. The simulated temperature level is, however, chosen lower than room temperature in order to minimize the fluctuations which are due to the thermal noise. A full understanding of the role of the temperature for the SSE is beyond the scope of this work.

We study the manipulation of the magnon accumulation by applying external magnetic fields. For this purpose, we simulate a system with $8 \times 8 \times 512$ spins including an easy axis parallel to the z direction with $d_z = 10^{-3}J$, a damping constant of $\alpha = 0.01$, and apply an external field in the z direction. Linear temperature gradients with variable lengths L excite net magnonic spin currents due to a nonequilibrium of the local magnonic density of states. In the hotter area more magnons exist than in the colder area and therefore more magnons propagate towards the colder region than the other way around, leading to a net magnon current from hot to cold. Since we aim to describe spin accumulation in samples with

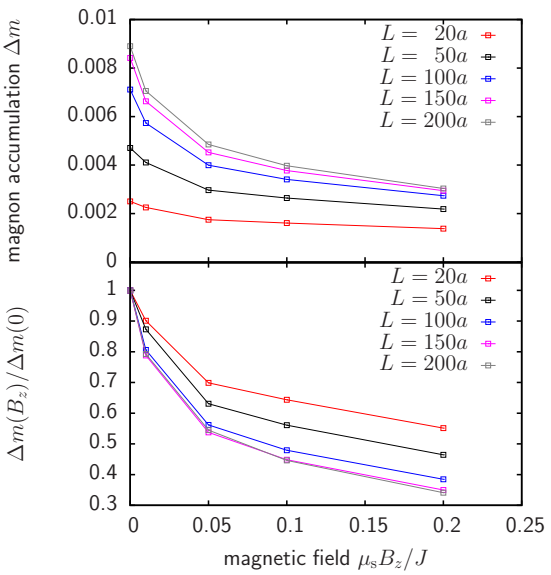

FIG. 2. (Color online) Upper part: Magnon accumulation at the cold end of the temperature gradient versus applied magnetic field B_z for different thicknesses with $\nabla T = 10^{-3}k_B T/(Ja)$, $\alpha = 0.01$, $d_z = 10^{-3}J$. Lower part: Corresponding normalized magnon accumulation $\Delta m(B)/\Delta m(0)$.

thin film geometry, we will call the spatial extension of the gradient L from now on the thickness.

After an initial relaxation the system reaches a quasistatic state where we calculate the local magnetization profile $m(z)$ as an average over time and over the x-y planes. The magnon accumulation can be defined as the difference of the local magnetization to its equilibrium value related to the local phonon temperature,

$$\Delta m(z) = m(z) - m_{eq}[T_p(z)]. \qquad (3)$$

Figure 1 shows exemplary the resulting magnon accumulation for an external field $B_z = 0.1J/\mu_s$ and a temperature gradient of $\nabla_z T = 10^{-3}J/(k_B a)$ for various thicknesses L. As shown in similar simulations by Kehlberger *et al.* the magnon accumulation has two extrema at the ends of the temperature gradient and their values increase with increasing thickness up to a characteristic length scale above which the magnon accumulation saturates. This characteristic length scale can be referred to as the mean magnon propagation length ξ_{avg} [7].

In the upper part of Fig. 2, the extreme value of the magnon accumulation at the cold end of the temperature gradient is shown versus applied magnetic field B_z for different thicknesses. The magnetic fields used in these simulations correspond to magnetic fields of the order of 80 T leading to strong effects. In all cases one can see that the magnon accumulation decreases with increasing field, but the observed suppression of the magnon accumulation is thickness dependent. For thicker films, larger than the mean magnon propagation length, the field suppression of the magnon accumulation is stronger than for thinner films where the suppression effect shows only a weak thickness dependence. This can be seen in the lower part of Fig. 2 where the normalized magnon accumulation $\Delta m(B_z)/\Delta m(0)$ is shown for various thicknesses.

The magnon accumulations at both the hot and the cold end of the temperature gradient are nearly proportional to the temperature difference between the magnonic and phononic subsystems [18]. It was shown by Xiao *et al.* that this temperature difference scales linearly with the spin Seebeck voltage, which is measured in experiments [17]. Hence, one can expect that the magnonic contribution to the SSE can be suppressed by magnetic fields. Interestingly, this behavior shows a thickness dependence with the influence of the field decreasing for thinner films, an effect that we will discuss later on.

First, in order to verify our theoretical model, the high magnetic field dependence of the SSE is measured using Pt/YIG hybrids. The samples used in the present study are (111)-oriented YIG slabs ($5 \times 10 \times 1$ mm^3) and YIG thin films grown on $Gd_3Ga_5O_{12}$ (GGG) substrate ($5 \times 10 \times 0.5$ mm^3) by liquid phase epitaxy. The thickness of the YIG thin films is varied from 0.3 to 50 μm. 5.5-nm-thick Pt layers are deposited on the YIG surfaces by dc-magnetron sputtering and further patterned into strips (length of 4 mm and width of 100 μm) by optical lithography and argon ion beam milling. Figure 3(a) shows a schematic diagram of the prepared sample and measurement setup. We adopt the longitudinal configuration to determine the SSE. The sample is sandwiched between the resistive heater and thermal sensor, further mounted onto a copper heat sink, then put into the cryostat. Each functional layer is structured on an Al_2O_3 substrate, which prevents an electrical short circuit of the individual elements, while ensuring maximal vertical temperature transport. Furthermore,

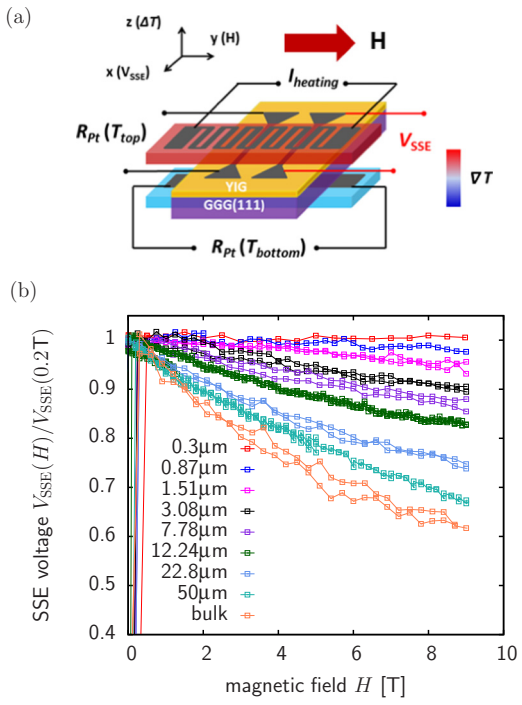

FIG. 3. (Color online) (a) Schematic diagram of sample structure and measurement setup. (b) Normalized spin Seebeck voltage $V_{SSE}(H)/V_{SSE}(0.2\,T)$ of Pt/YIG structures composed of YIG single crystal and selected YIG thin films with thickness ranging from 0.3 to 50 μm.

a thermal grease is used for the mounting of the elements, which ensures good thermal connection at the interfaces. A temperature gradient ∇T can be generated by the attached resistive heater and be varied by simply changing the heating currents. A spin current is thermally generated in the Pt layer along the direction of thermal gradient (z axis), and further converted into an electric field due to the inverse spin Hall effect. The SSE can be detected electrically by measuring the voltage drop V_{SSE} at the two ends of the Pt strip (along the x axis). The benefit of our measurement setup is that the Pt strips on the top and bottom surfaces of the samples can be utilized as an excellent resistance-temperature detector to determine the temperature differences across the hybrids precisely. In our room-temperature experiments we keep the cryostat at a fixed temperature of 300 K and a heating current in our resistive heater of $I_{heat} = 9$ mA results in the temperature difference ΔT of roughly 4.2 ± 0.2 K for our measurements. An external magnetic field H is applied perpendicular to the Pt strip along the y axis. The maximum magnetic field is up to 9 T, which is orders of magnitude higher than the coercivity of YIG, ensuring that the magnetization of the YIG slab (or YIG thin films) is well aligned along the field direction. To exclude proximity effects from the Pt/YIG interface as the origin of the observed field suppression of the SSE, the magnetoresistance of the Pt layer is monitored, which shows no noticeable change beyond the saturation field of magnetization of the YIG film.

The V_{SSE} is recorded as a function of magnetic fields. The SSE signal appears when a magnetic field is applied and flips its sign when the field reverses. We find the magnitude of the SSE signal suppressed by high magnetic fields at room temperature. The maximum value of V_{SSE} is found at the smallest field interval of 0.2 T. The thickness dependent SSE coefficient $\sigma_{SSE} = V_{SSE}(0.2\,T)/\Delta T$ exhibits a similar trend to the one observed in our previous work: the σ_{SSE} is enhanced with increasing film thickness and saturates above a characteristic length, demonstrating the bulk origin of magnonic spin current [7]. Figure 3(b) shows examples of the normalized spin Seebeck voltages $V_{SSE}(H)/V_{SSE}(0.2\,T)$ for selected Pt/YIG hybrids. In agreement with the numerical simulations, the experiments show a nonlinear behavior of the suppression with increasing magnetic fields and a strong thickness dependence of the suppression effect. Using a magnetic moment of $\mu_s = 2.2 \times 10^{-22}$ J/T which corresponds to a magnetization of $M_s = 140$ kA/m [7] for a unit cell with a lattice constant $a = 1.2$ nm and an exchange constant $J = 5.4 \times 10^{-21}$ J derived from a critical temperature of $T_C = 550$ K [15], the simulation of $\mu_s B_z = 0.2J$ corresponds to a magnetic field of about 4.5 T. In experiments a suppression of 30% was observed, whereas the simulations for $L = 200a$ show a suppression of 60%. This deviation appears probably due to the lower temperature used in the simulations and the limitations of the ferromagnetic approach for YIG. This suppression drops in the experiments to only 0.1% for 0.3-μm-thick YIG films. In simulations a reduction of the suppression is also observed, but here the effect is weaker. In the thinnest samples of the experiments the low frequency magnons are strongly suppressed due to the finite sample thickness and therefore the magnetic field suppression of the SSE is practically vanishing. In our simulations the region with the temperature

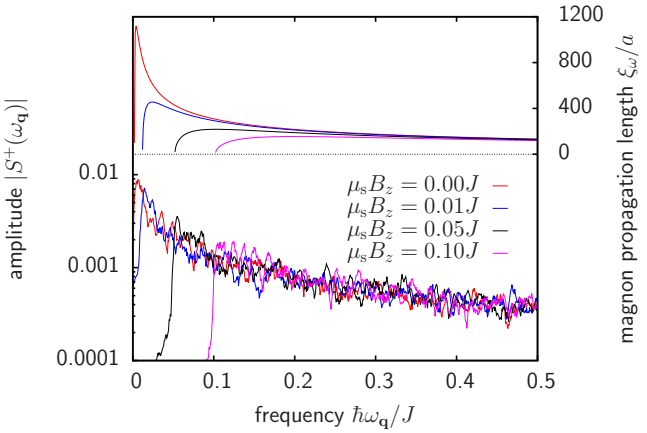

FIG. 4. (Color online) Magnon frequency distribution of propagating magnons at the cold end of the temperature gradient and the frequency dependent magnon propagation length for different magnetic fields.

gradient is connected with a perfect heat source, without cutoff. Nevertheless, the suppression is decreasing in agreement with the experimental observations.

To understand the suppression effect at a fundamental level, we analyze it next based on an analytical linear spin wave theory. In particular, we determine in this model the origin of the field suppression of the magnon accumulation as well as the thickness dependence of this effect. The magnonic dispersion relation of the simulated system can be calculated by solving the linearized LLG equation,

$$\hbar\omega_\mathbf{q} = 2d_z + \mu_s B_z + 2J \sum_\theta [1 - \cos(q_\theta a_\theta)], \qquad (4)$$

where θ denotes the spatial coordinates x, y, z. The dispersion relation consists of a magnon frequency gap $\hbar\omega_{\min} = (2d_z + \mu_s B_z)$ and a second term depending on the wave vector $\mathbf{q}$. The frequency gap, which in the absence of magnetic fields, is given by the anisotropy, increases linearly with increasing magnetic fields and, hence, parts of the spectrum are frozen out for higher magnetic fields. This effect can be seen in Fig. 4. By calculating a Fourier transformation of the magnon accumulation Δm in the time domain, as used by Ritzmann *et al.* [18], at the cold end of the temperature gradient, we can calculate the frequency distribution of the magnons from our simulations. The shown frequency distributions for temperature gradients with width $L = 200a$ for different magnetic fields shows a clear shift of the frequency gap and therefore a suppression of parts of the frequency spectra. This effect can explain the suppression of the accumulation due to applied magnetic fields.

The frequency dependent magnon propagation length $\xi(\omega)$ is also shown in Fig. 4. It can be estimated using the lifetime $\tau = (\alpha\omega)^{-1}$ and the group velocity of the magnons [18] leading to the expression

$$\frac{\xi_{\omega_\mathbf{q}}}{a} = \frac{\sqrt{J^2 - \left[\frac{1}{2}(\hbar\omega_q - \hbar\omega_{\min}) - J\right]^2}}{\alpha\hbar\omega_\mathbf{q}}. \qquad (5)$$

The maximum propagation length is given by

$$\frac{\xi_{\max}}{a} = \frac{1}{\sqrt{2}\alpha}\sqrt{\frac{J}{\hbar\omega_{\min}}} \qquad (6)$$

and can be much larger than the mean propagation length of the magnons.

The thickness dependence of the field suppression can be explained by the frequency dependent magnon propagation length. Magnons with large propagation length will always reach the cold end of the temperature gradient. When the thickness is reduced, the contribution of those magnons is reduced. Since only these magnons are suppressed by the frequency gap, the field suppression is also reduced for low thicknesses. Note that the equations above show that the same suppression effect would appear by modifying the anisotropy in the system, since the effect depends not only on the size of the magnetic field, but on the value of the frequency gap.

Furthermore, not only parts of the spectrum are suppressed, but also the frequency dependent magnon propagation length $\xi(\omega)$ is modified by applying higher magnetic fields. When the propagation length of the magnons is reduced, the number of magnons propagating through the system is smaller, leading also to a reduction of the magnon accumulation, showing that multiple effects contribute to this generic property of thermal magnon propagation in applied magnetic fields.

In conclusion, we have shown numerical simulations and experiments on the magnetic field suppression of the longitudinal SSE. Applying large magnetic fields can suppress the excited magnon spin currents by suppressing parts of the frequency spectrum. We find qualitative agreement between the performed simulation and experiments of the field dependence of the longitudinal SSE in YIG at room temperature for various thicknesses. The suppression is strongly dependent on the thickness of the sample and is practically vanishing for thin films since low frequency magnons play a minor role in thin films as compared to bulk materials. Furthermore, not only parts of the spectra are suppressed but the magnon propagation length given by the Gilbert damping is modified leading to a lower propagation length in systems with higher magnetic fields. Our analysis opens a new avenue to determining which magnons contribute to the spin current as a careful study of the field dependence would allow then to measure the intensities of the involved frequency as proposed by Boona *et al.* [21]. Furthermore, the field suppression open new opportunities for the control of the magnon flow and resulting SSE with external fields. During the preparation of this paper we became aware of two related experimental works [25,26] supporting our findings.

The authors would like to thank the Deutsche Forschungsgemeinschaft for financial support via SPP 1538 "Spin Caloric Transport" and the SFB 767 "Controlled Nanosystem: Interaction and Interfacing to the Macroscale" as well as the EU (IFOX, NMP3-LA-2012246102, INSPIN, FP7-ICT-2013-X 612759, MASPIC, ERC-2007-StG 208162).

[1] G. E. W. Bauer, E. Saitoh, and B. J. van Wees, Nat. Mater. **11**, 391 (2012).
[2] S. R. Boona, R. C. Myers, and J. P. Heremans, Energy Environ. Sci. **7**, 885 (2014).
[3] E. Saitoh, M. Ueda, H. Miyajima, and G. Tatara, Appl. Phys. Lett. **88**, 182509 (2006).
[4] S. O. Valenzuela and M. Tinkham, Nature (London) **442**, 176 (2006).
[5] K. Uchida, H. Adachi, T. Ota, H. Nakayama, S. Maekawa, and E. Saitoh, Appl. Phys. Lett. **97**, 172505 (2010).
[6] M. Weiler, M. Althammer, F. D. Czeschka, H. Huebl, M. S. Wagner, M. Opel, I.-M. Imort, G. Reiss, A. Thomas, R. Gross, and S. T. B. Goennenwein, Phys. Rev. Lett. **108**, 106602 (2012).
[7] A. Kehlberger, U. Ritzmann, D. Hinzke, E.-J. Guo, J. Cramer, G. Jakob, M. C. Onbasli, D. H. Kim, C. A. Ross, M. B. Jungfleisch, B. Hillebrands, U. Nowak, and M. Kläui, Phys. Rev. Lett. **115**, 096602 (2015).
[8] M. Schreier, A. Kamra, M. Weiler, J. Xiao, G. E. W. Bauer, R. Gross, and S. T. B. Goennenwein, Phys. Rev. B **88**, 094410 (2013).
[9] T. Kikkawa, K. Uchida, Y. Shiomi, Z. Qiu, D. Hou, D. Tian, H. Nakayama, X.-F. Jin, and E. Saitoh, Phys. Rev. Lett. **110**, 067207 (2013).
[10] T. Kikkawa, K. Uchida, S. Daimon, Y. Shiomi, H. Adachi, Z. Qiu, D. Hou, X.-F. Jin, S. Maekawa, and E. Saitoh, Phys. Rev. B **88**, 214403 (2013).
[11] M. Schreier, N. Roschewsky, E. Dobler, S. Meyer, H. Huebl, R. Gross, and S. T. B. Goennenwein, Appl. Phys. Lett. **103**, 242404 (2013).
[12] M. Agrawal, V. I. Vasyuchka, A. A. Serga, A. Kirihara, P. Pirro, T. Langner, M. B. Jungfleisch, A. V. Chumak, E. T. Papaioannou, and B. Hillebrands, Phys. Rev. B **89**, 224414 (2014).
[13] N. Roschewsky, M. Schreier, A. Kamra, F. Schade, K. Ganzhorn, S. Meyer, H. Huebl, S. Geprägs, R. Gross, and S. T. B. Goennenwein, Appl. Phys. Lett. **104**, 202410 (2014).
[14] N. Vlietstra, J. Shan, B. J. van Wees, M. Isasa, F. Casanova, and J. Ben Youssef, Phys. Rev. B **90**, 174436 (2014).
[15] K.-i. Uchida, T. Kikkawa, A. Miura, J. Shiomi, and E. Saitoh, Phys. Rev. X **4**, 041023 (2014).
[16] S. Y. Huang, X. Fan, D. Qu, Y. P. Chen, W. G. Wang, J. Wu, T. Y. Chen, J. Q. Xiao, and C. L. Chien, Phys. Rev. Lett. **109**, 107204 (2012).
[17] J. Xiao, G. E. W. Bauer, K.C. Uchida, E. Saitoh, and S. Maekawa, Phys. Rev. B **81**, 214418 (2010).
[18] U. Ritzmann, D. Hinzke, and U. Nowak, Phys. Rev. B **89**, 024409 (2014).
[19] S. Hoffman, K. Sato, and Y. Tserkovnyak, Phys. Rev. B **88**, 064408 (2013).
[20] S. R. Etesami, L. Chotorlishvili, A. Sukhov, and J. Berakdar, Phys. Rev. B **90**, 014410 (2014).
[21] S. R. Boona and J. P. Heremans, Phys. Rev. B **90**, 064421 (2014).
[22] D. Landau and E. Lifshitz, Phys. Z. Sowjetunion **8**, 153 (1935).
[23] T. Gilbert, Phys. Rev. **100**, 1243 (1955).
[24] U. Nowak, *Handbook of Magnetism and Advanced Magnetic Materials*, edited by Helmut Kronmüller and Stuart Parkin, Vol. 2: Micromagnetism (John Wiley and Sons, New York, 2007).
[25] T. Kikkawa, K.-i. Uchida, S. Daimon, Z. Qiu, Y. Shiomi, and E. Saitoh, Phys. Rev. B **92**, 064413 (2015).
[26] H. Jin, S. R. Boona, Z. Yang, R. C. Myers, and J. P. Heremans, Phys. Rev. B **92**, 054436 (2015).